International Journal of Chemical, Materials and Biomolecular Sciences
ISSN: 2415-6620
Vol:13, No:2, 2019

Uncertainty Analysis of ROSA/LSTF Test on Pressurized Water Reactor Cold Leg Small-Break Loss-of-Coolant Accident without Scram

Takeshi Takeda

***Abstract*—**The author conducted post-test analysis with the RELAP5/MOD3.3 code for an experiment using the ROSA/LSTF (rig of safety assessment/large-scale test facility) that simulated a 1% cold leg small-break loss-of-coolant accident under the failure of scram in a pressurized water reactor. The LSTF test assumed total failure of high-pressure injection system of emergency core cooling system. In the LSTF test, natural circulation contributed to maintain core cooling effect for a relatively long time until core uncovery occurred. The post-test analysis result confirmed inadequate prediction of the primary coolant distribution. The author created the phenomena identification and ranking table (PIRT) for each component. The author investigated the influences of uncertain parameters determined by the PIRT on the cladding surface temperature at a certain time during core uncovery within the defined uncertain ranges.

***Keywords*—**LSTF, LOCA, scram, RELAP5.

I. Introduction

SMALL amounts of boron residue and cracks were found around the circumference of penetration nozzles for the control rod drive mechanism in the vessel upper head of the Oconee Unit-3 of pressurized water reactor (PWR) in the US [1]. Cuadra et al. [2] have presented the notion that the core would remain subcritical if 4-inch diameter break happens in the vessel upper head under the failure of scram, through the calculation for the Oconee Unit-3 by employing a coupled three-dimensional kinetics and thermal-hydraulic code. There have been scarcely any experimental studies on PWR small-break loss-of-coolant accident (SBLOCA) without scram. An experiment denoted as SB-CL-38 simulated a PWR SBLOCA with 1% cold leg break under the high-power condition due to the failure of scram utilizing the ROSA/LSTF [3] of Japan Atomic Energy Agency in 2006. The LSTF test assumed total failure of high-pressure injection system of emergency core cooling system adverse to the core cooling.

In the author's previous work [4], the post-test analysis of the LSTF test was carried out by employing the RELAP5/MOD3.2 code in which a fine-mesh single flow channel model and simple core model respectively, were represented by the steam generator (SG) medium tube and by the mean-power rod bundle. The results suggested the necessity of further evaluating the code predictive capability. In this follow-up study, first, the author assessed the LSTF test by using the RELAP5/MOD3.3 code [5] with a fine-mesh multiple parallel flow channel model for the SG U-tubes to better predict nonuniform flow behavior among the U-tubes. At that time, the core was modeled being the consideration of the cross-flow between different power rod bundles for better representation of multi-dimensional flow in the core. Meanwhile, some researchers [6], [7] have analyzed the LSTF test by employing the RELAP5 and TRACE codes but with no uncertainty evaluation. In this follow-up study, next, the author tried to ensure PIRT for each component. In the LSTF test, the core power automatically decreased to protect the core because the maximum cladding surface temperature of the simulated fuel rods exceeded the predetermined criterion of 873 K (to be presented in Fig. 8). The automatic core power reduction affected significantly peak cladding temperature. The PIRT was thus set up in view of the importance of phenomena in determining not the peak cladding temperature, but the cladding surface temperature at a certain time during core uncovery. The PIRT was established based on the LSTF test data analysis and the post-test analysis. Finally, the author performed sensitivity and uncertainty analyses of the LSTF test with the RELAP5 code to study the influences of uncertain parameters determined by the PIRT on the cladding surface temperature at a certain time during core uncovery. This paper describes major consequences from the LSTF test and the RELAP5 code analyses.

Takeshi Takeda is with Nuclear Regulation Authority, Roppongi, Minato-ku, Tokyo 106-8450, Japan (phone: 81-3-5114-2100; fax: 81-3-5114-2178; e-mail: takeda.takeshi4695@gmail.com).

II. ROSA/LSTF

The ROSA/LSTF simulates a Westinghouse-type four-loop 3,423 MW (thermal) PWR, which is represented by a two-loop system with full-height and 1/48-scaled volume of the reference PWR of Tsuruga Unit-2. As shown schematically in Fig. 1, the LSTF consists of a pressure vessel, pressurizer (PZR), and primary loops. An active SG, primary coolant pump, and hot and cold legs are included in each loop. Each SG has 141 full-size U-tubes with 19.6 mm in inner-diameter and nine different lengths, as mentioned in Table I. There are inlet and outlet plena, boiler section, steam separator, steam dome, steam dryer, main steam line, four downcomer pipes, and other internals for each SG. Six instrumented tubes for each SG are composed of two short tubes (Type 1 in Table I) denoted as Tubes 1 and 6, two medium tubes (Type 5) as Tubes 2 and 5, and two long tubes (Type 9) as Tubes 3 and 4. The hot and cold legs with 207 mm in inner-diameter of each are sized to conserve the volumetric scale (2/48) as well as the ratio of the length to the square root of the pipe diameter [8]. This approach is taken to

better simulate the flow regime transitions in the primary loops. The core (active height of 3.66 m) consists of 1,008 electrically heated rods in 24 rod bundles as the simulated fuel rod assembly of the reference PWR. The axial profile of the core power is structured in a nine-step chopped cosine where a peaking factor is 1.495. The LSTF initial core power is 10 MW, which is 14% of the volumetric-scaled (1/48) nominal core power of the reference PWR.

TABLE I
DETAILS OF LSTF U-TUBES IN EACH SG

Type	Straight Length (m)	Number of Tubes	Instrumented Tubes
1	9.44	21	Two short tubes
2	9.59	19	
3	9.74	19	
4	9.89	19	
5	10.04	17	Two medium tubes
6	10.19	15	
7	10.39	13	
8	10.49	11	
9	10.64	7	Two long tubes

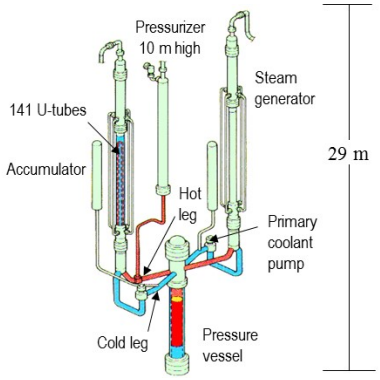

Fig. 1 Schematic view of ROSA/LSTF

III. LSTF TEST AND RELAP5 CODE ANALYSIS CONDITIONS

A. LSTF Test Conditions

The break was simulated by using a 10.1 mm inner-diameter, sharp-edge orifice, horizontally mounted flush with the cold leg inner surface in a loop without PZR. The orifice size corresponds to 1% of the volumetrically-scaled cross-sectional area of the reference PWR cold leg. The experiment was launched at time zero by opening a break valve located downstream of the break orifice. Initial PZR pressure was set to 15.5 MPa according to the reference PWR conditions. Initial SG secondary-side pressure of 7.3 MPa was caused by the limitation of the primary-to-secondary heat transfer rate of 10 MW. The SG secondary-side pressure of 8.03 MPa and 7.82 MPa corresponded to set point pressure for opening and closure of SG relief valves, respectively, by reference to the set point value used in the reference PWR. The core power curve for the LSTF test was predetermined through the calculation for a PWR 1% cold leg SBLOCA without scram under an assumption of totally failed high-pressure injection system by utilizing the SKETCH-INS/TRAC-PF1 code [9]. The LSTF core power was kept constant at 10 MW for 203 s until the scaled PWR core decay power dropped to 10 MW. The coastdown of the primary coolant pumps and the auxiliary feedwater injection into the secondary-side of SGs were supposed to start concurrently with a scram signal at 20 s, on the basis of the code calculation for the PWR SBLOCA without scram. The core power was reduced to a certain low level in several steps to protect the core because the maximum cladding surface temperature was above 873 K.

B. RELAP5 Calculation Conditions

The employed code for the calculations of the LSTF test was the RELAP5/MOD3.3 code with a two-phase critical flow model, which may correctly predict the discharge rate through the sharp-edge orifice to simulate the break. The model uses the Bernoulli incompressible orifice flow equation for single-phase discharge liquid [10]. The maximum bounding flow theory was applied to two-phase discharge flow [11]. Values of the discharge coefficient (C_d) of 0.61, 0.61, and 0.84 respectively, were employed for single-phase discharge liquid, two-phase discharge flow, and single-phase discharge steam [12].

Fig. 2 (a) indicates the overall schematic of the LSTF system for the RELAP5 code analysis. One-dimensional model of the LSTF system included a pressure vessel, primary loops, PZR, SGs, and SG secondary-side system. Nine parallel flow channels corresponding to the nine different lengths of U-tubes for each SG were used to better predict the nonuniform flow behavior among the SG U-tubes (to be presented in Fig. 6). Specifically, each of four short-to-medium tubes with straight lengths of 9.44–9.89 m (Table I) was represented by 24 nodes, and each of five medium-to-long tubes with straight lengths of 10.04–10.64 m (Table I) was divided into 26 nodes.

As indicated in Fig. 2 (b), the core was represented by three vertical stacks of nine equal-height volumes, according to a nine-step chopped cosine power profile along the length of the core. The stack of the high-power rod bundle was horizontally connected to that of the mean-power rod bundle by nine cross-flow junctions and to that of the low-power rod bundle by nine cross-flow junctions based on the core configuration, for better representation of multi-dimensional flow in the core. Each stack was composed of components for fluid and heat structures, and was connected to branches at the core inlet and exit. Input data set included the radial core power distribution taking into account the peaking factor and the number of high-, mean-, and low-power rod bundles.

To simulate counter-current flow limiting (CCFL) at the SG U-tube inlet and inlet plenum bottom (to be shown in Fig. 6); the author applied the following correlation of Wallis [13].

$$j_G^{*1/2} + m j_L^{*1/2} = C, \quad (1)$$

where j^* is the dimensionless volumetric flux. Gas and liquid phases are denoted by subscripts G and L, respectively. Slope m and intercept C of the Wallis CCFL correlation in the SG U-tube inlet represented by the junction connecting component for the SG U-tube to that for the SG inlet plenum were given as 1 and 0.75, respectively, referring to a separate-effect test with

the LSTF focusing on the CCFL at the SG U-tube inlet [14]. Slope m and intercept C of the Wallis CCFL correlation in the SG inlet plenum bottom represented by the junction connecting component for the SG inlet plenum to that for the hot leg were set to 1 and 0.8 respectively as trial values because of no empirical constants of the CCFL correlation depending on flow channel structure. In the calculation only, no automatic decrease in the core power was made when the maximum cladding surface temperature exceeded 873 K. Other initial and boundary conditions employed were in accordance with the LSTF test conditions.

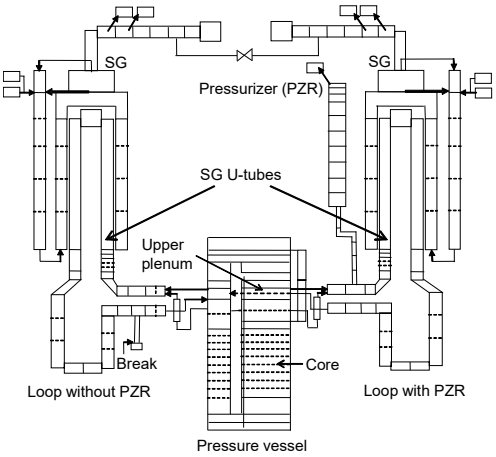

(a)

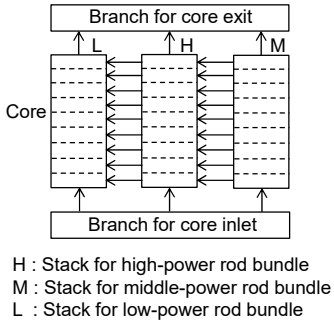

(b)

Fig. 2 (a) Overall schematic of LSTF system and (b) details of LSTF core as noding schematic of LSTF for RELAP5 code analysis

IV. LSTF Test and RELAP5 Code Analysis Results

A. Major Phenomena Observed in the Experiment

Figs. 3–8 show the major phenomena observed in the LSTF test. Single-phase break flow changed to two-phase break flow at about 300 s when a significant drop appeared in the cold leg liquid level (Fig. 3). This resulted in a decrease in the break flow rate. The SG relief valves were kept open at about 80–300 s, and the cycle opening of the relief valves occurred three times due to high core power thereafter (Fig. 4). The primary pressure became closer to the SG secondary-side pressure with time after the termination of the cycle opening of the SG relief valves (Fig. 4).

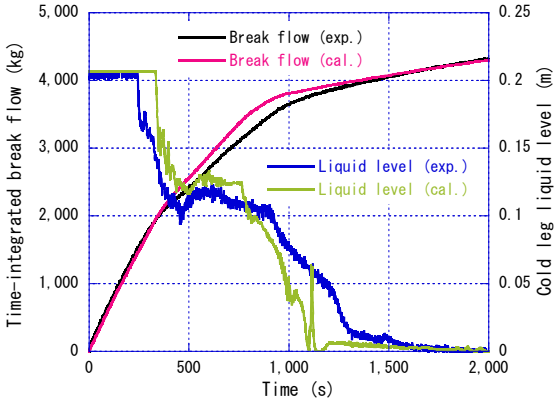

Fig. 3 Test and calculated results for break flow and cold leg liquid level in loop without PZR

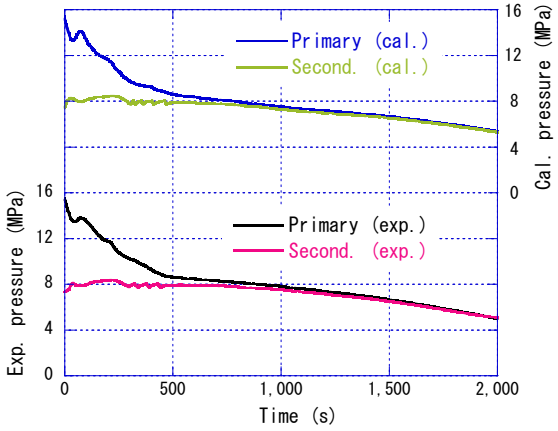

Fig. 4 Test and calculated results for primary and SG secondary-side pressures in loop with PZR

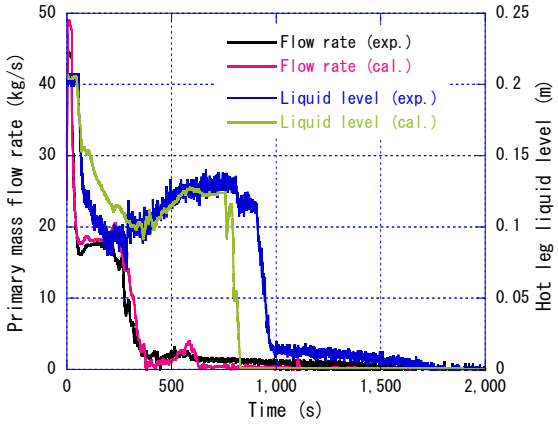

Fig. 5 Test and calculated results for primary mass flow rate and hot leg liquid level in loop with PZR

Liquid levels in the hot legs became quite low because of supercritical flow in the hot legs due to high velocity steam and liquid flows (Fig. 5). Natural circulation (NC) mode changed

from two-phase NC to reflux condensation at around 300 s, which resulted in the liquid recovery in the hot legs (Fig. 5). The collapsed liquid levels in the SG U-tube upflow-side were different from each other until around 500 s (Fig. 6). Liquid was accumulated in the U-tube upflow-side and inlet plena of SGs during reflux condensation because of the CCFL for high steam velocity (Fig. 6). A significant level drop in the hot leg began at about 900 s after the SG inlet plenum became empty of liquid (Figs. 5 and 6). Core uncovery took place by core boil-off after the upper plenum became voided at the primary pressure of about 7 MPa (Figs. 7 and 8).

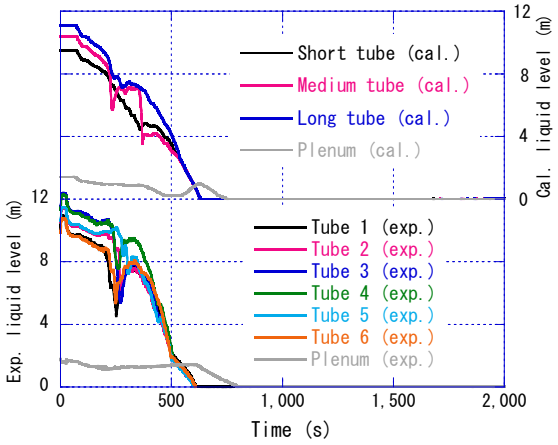

Fig. 6 Test and calculated results for collapsed liquid levels in SG inlet plenum and U-tube upflow-side in loop with PZR

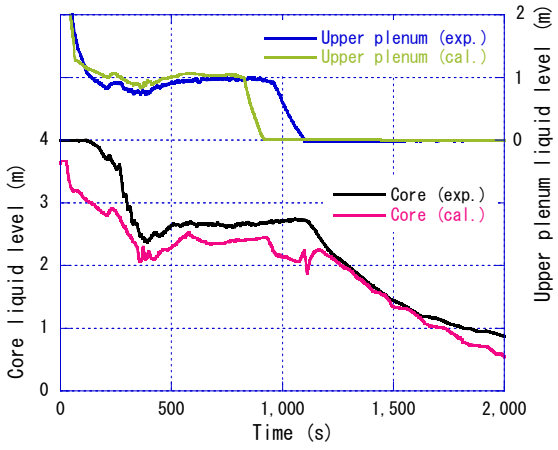

Fig. 7 Test and calculated results for upper plenum and core collapsed liquid levels

The automatic reduction was actuated in the core power at about 1,620 s because the maximum cladding surface temperature exceeded 873 K (Fig. 8). The measuring points at Positions 6, 7, and 8 respectively, are located at about 2.2 m, 2.6 m, and 3.0 m above the core bottom, while the locations of the nodes of Positions 6, 7, and 8 respectively correspond to about 2.0–2.4 m, 2.4–2.8 m, and 2.8–3.2 m above the core bottom mentioned later. The peak cladding temperature observed at Position 7 was 904 K at about 1,820 s. This suggested that an intentional primary depressurization, e.g. through SG secondary-side depressurization by fully opening the SG secondary valves [15], should be essential for long-term core cooling by coolant injection from the emergency core cooling system in this type of SBLOCA under the failure of scram.

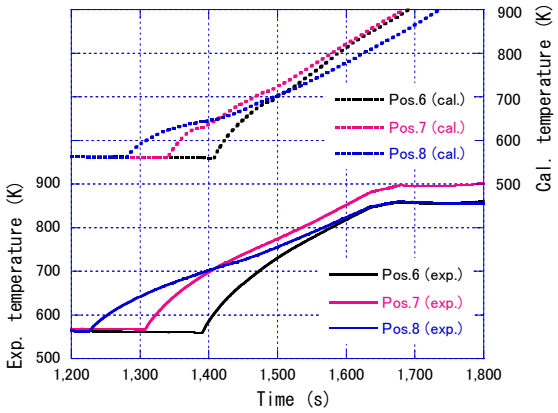

Fig. 8 Test and calculated results for cladding surface temperature

B. Comparison of Calculated Results with LSTF Test Data

The RELAP5 code calculated the overall trends of the major thermal-hydraulic responses observed in the LSTF test well. However, the break flow rate was overpredicted during two-phase flow discharge period (Fig. 3). This was probably due to insufficient prediction of the cold leg liquid level during two-phase NC and reflux condensation. Owing to the overprediction of the break flow rate, the upper plenum as well as the hot and cold legs became empty of liquid earlier in the calculation compared to the LSTF test (Figs. 3, 5, and 7), and the primary pressure was underpredicted (Fig. 4). The primary mass flow rate was overpredicted because a significant level drop in the cold leg began later in the calculation compared to the LSTF test (Figs. 3 and 5). Supercritical flow in the hot legs was well calculated, though with a tendency that the hot leg liquid level was overpredicted (Fig. 5). Liquid accumulation in the U-tube upflow-side and inlet plena of SGs was well calculated, though with tendencies that the collapsed liquid levels in the SG U-tube upflow-side and inlet plena were underpredicted (Fig. 6). The calculated result reproduced the liquid level change with some randomness among the SG U-tubes (Fig. 6). This suggested that detailed modeling of the SG U-tubes with fine-mesh multiple parallel flow channels should be required where such nonuniform flow happens among the SG U-tubes. The core uncovery by core boil-off started later in the calculation compared to the LSTF test due to inadequate prediction of the core liquid level drop (Figs. 7 and 8). The trends of the cladding surface temperatures at the nodes of Positions 6, 7, and 8 in the calculation agreed reasonably well with those at the corresponding positions in the LSTF test, but the cladding surface temperature was underpredicted until the actuation of the automatic core power decrease after the core uncovery initiation in the LSTF test (Fig. 8).

V. Sensitivity and Uncertainty Analyses

A. Sensitivity and Uncertainty Analysis Conditions

Table II shows the PIRT and related uncertain parameters. Each phenomenon is granted a ranking of high, medium, or low. High-, medium-, and low-ranked phenomena respectively, may have large, medium, and small effects on the cladding surface temperature at a certain time during core uncovery. The high-ranked phenomena included critical flow at the break, decay heat of the fuel rods, core two-phase mixture level, core heat transfer, and steam discharge through the SG relief valve. Liquid accumulation in the SG U-tube upflow-side and inlet plena was regarded as the medium-ranked phenomena. The reason for this was because the SG U-tube upflow-side and inlet plena became empty of liquid prior to the initiation of core uncovery. Two-phase mixture levels in the upper plenum and the downcomer, stored heat of the fuel rods, core rewet, and supercritical flow in the hot leg were also included in the medium-ranked phenomena. The other phenomena corresponded to the low-ranked phenomena.

TABLE II
PIRT and Related Uncertain Parameters

Component	Phenomenon	Rank*	Parameter
Break	Critical flow	H	Break discharge coefficient for single-phase liquid and two-phase flow
Upper head	Two-phase mixture level	L	Gas-liquid inter-phase drag in upper head
Upper plenum	Two-phase mixture level	M	Gas-liquid inter-phase drag in upper plenum
	Horizontal stratification	L	Gas-liquid relative velocity in cold leg
Fuel rods	Decay heat	H	Core decay power
	Stored heat	M	Thermal conductivity of fuel rod
			Heat capacity of fuel rod
Core	Two-phase mixture level	H	Gas-liquid inter-phase drag in core
	Heat transfer	H	Film boiling and steam convective heat transfer coefficients in core
	Rewet	M	Boiling heat flux in core
Downcomer	Two-phase mixture level	M	Gas-liquid inter-phase drag in downcomer
	Bypass flow between upper head and downcomer	L	Form loss coefficient in upper head spray nozzle
	Bypass flow between hot leg leak line and downcomer	L	Form loss coefficient in hot leg nozzle
Pressurizer	Two-phase mixture level	L	Gas-liquid inter-phase drag in pressurizer
Hot leg	Supercritical flow	M	Liquid velocity in hot leg
	Horizontal stratification	L	Gas-liquid relative velocity in hot leg
SG	Liquid accumulation in SG U-tube upflow-side and inlet plena	M	Slope *m* of Wallis CCFL correlation in SG U-tube inlet Intercept *C* of Wallis CCFL correlation in SG U-tube inlet Slope *m* of Wallis CCFL correlation in SG inlet plenum bottom Intercept *C* of Wallis CCFL correlation in SG inlet plenum bottom
	Steam discharge through SG secondary valve	H	Discharge coefficient through SG relief valve
Crossover leg	Horizontal stratification	L	Gas-liquid relative velocity in crossover leg
Cold leg	Horizontal stratification	L	Gas-liquid relative velocity in cold leg
Primary coolant pump	Flow resistance	L	Resistance coefficient in primary coolant pump
	Coastdown performance	L	Rotation speed of primary coolant pump

* H, high-ranked phenomenon; L, low-ranked phenomenon; M, medium-ranked phenomenon

Table III shows the uncertain parameters and ranges applicable to the high-ranked phenomena. The C_d through the break for single-phase liquid and two-phase flow was in the range of 0.60 to 0.62; these values were used to clarify the effects of small differences in the C_d on the cladding surface temperature. The range of the core decay power was the specified value ±0.07 MW, which is the same as the measurement uncertainty [3]. In the RELAP5 code, the gas-liquid inter-phase drag model in the core is based on the work on the interfacial area and the drag in the circular pipe geometry [16]. The gas-liquid inter-phase drag in the core ranged from 50% to 150%; these values were set to make clear the effects of relatively large differences in the inter-phase drag on the cladding surface temperature, referring to the related analytical approach [17]. The film boiling heat transfer is estimated at the correlations [18], [19]. The convective heat transfer by the steam flow is evaluated from the maximum value among the correlation-based estimation values [20]-[22]. The film boiling and steam convective heat transfer coefficients in the core were in the range of 50% to 150%; these values were used to clarify the effects of relatively large differences in the heat transfer coefficients on the cladding surface temperature. The C_d through the SG relief valve ranged from 0.74 to 0.94; these values were set to make clear the effects of relatively large differences in the C_d on the cladding surface temperature.

The ranges of the core decay power, the gas-liquid inter-phase drag in the core, and the film boiling and steam convective heat transfer coefficients in the core were due to the measurement uncertainty or the unknown uncertainty of the physical models in the RELAP5 code, and thus the distribution for the three uncertain parameters was regarded as the normal distribution. The C_d through the SG relief valve as well as the C_d through the break for single-phase liquid and two-phase flow affected the predictive capability of the RELAP5 code for such phenomena as critical flow and steam discharge through the SG relief valve, and thus the distribution for the two

uncertain parameters was considered as the uniform distribution.

To determine the necessary number n of the computer code runs, the author applied the following formula for the pth order by Guba et al. [23].

$$\sum_{j=0}^{n-p} \frac{n!}{(n-j)!\,j!} \alpha^{j} (1-\alpha)^{n-j} \geq \beta, \qquad (2)$$

where α is the probability and β is the confidence level. The author selected 124 cases as the required number of the computer code calculations for a 95% probability and 95% confidence level, and the third order. This selection referred to the lesson learned from the uncertainty analyses of the large-break LOCA test of the LOFT (loss of fluid test) [24]. For 124 cases, a random value for each set of the uncertain parameters was generated by the Latin hypercube sampling method [25], which served as an efficient sampling technique for various kinds of uncertainty analyses [26].

TABLE III
UNCERTAIN PARAMETERS AND RANGES

Parameter	Base Case Value	Range	Distribution
Discharge coefficient through break for single-phase liquid and two-phase flow	0.61	[0.60, 0.62]	Uniform
Core decay power	Specified value MW	[–0.07, +0.07]MW	Normal
Gas-liquid inter-phase drag in core	100%	[50, 150]%	Normal
Film boiling and steam convective heat transfer coefficients in core	100%	[50, 150]%	Normal
Discharge coefficient through SG relief valve	0.84	[0.74, 0.94]	Uniform

B. Sensitivity and Uncertainty Analysis Results

Figs. 9–13 compare the results of the sensitivity analysis and the post-test analysis (base case calculation) for the cladding surface temperature at the node of Position 7, where the temperature at 1,600 s was the highest among the nodes, in terms of each uncertain parameter. The time of 1,600 s was just before the actuation of the automatic core power decrease in the LSTF test. The cladding surface temperature started to increase later when the C_d value through the break was 0.60, while this temperature began to rise earlier in the case of the C_d value of 0.62, as compared to the base case of 0.61 (Fig. 9). The cladding surface temperature at 1,600 s was lower for a value of C_d of 0.60, while it was higher for a value of the C_d of 0.62, as opposed to the base case of 0.61. The cladding surface temperature at 1,600 s may be considerably higher when the C_d through the break is somewhat larger. As for the core decay power, the cladding surface temperature started to increase later in the case of the specified value minus 0.07 MW, while it began to rise earlier in the case of the specified value plus 0.07 MW, as compared to the base case of the specified value (Fig. 10). The cladding surface temperature at 1,600 s was lower in the case of the specified value minus 0.07 MW, while it was higher in the case of the specified value plus 0.07 MW, as opposed to the base case of the specified value. The cladding surface temperature at 1,600 s may be significantly higher when the core decay power is somewhat larger. Regarding the gas-liquid inter-phase drag in the core, the cladding surface temperature started to increase later in the case of a value of 50%, while it began to rise earlier in the case of a value of 150%, as compared to the base case of 100% (Fig. 11). The cladding surface temperature at 1,600 s was higher in the case of a value of 50%, while it was lower in the case of a value of 150%, as opposed to the base case of 100%. The cladding surface temperature at 1,600 s may be substantially higher when the core inter-phase drag is somewhat smaller. Concerning the film boiling and steam convective heat transfer coefficients in the core, the cladding surface temperature at 1,600 s was higher in the case of a value of 50%, while it was lower in the case of a value of 150%, as compared to the base case of 100% (Fig. 12). The cladding surface temperature at 1,600 s may be relatively higher when the film boiling and steam convective heat transfer coefficients in the core are somewhat smaller. There was no apparent relationship between the C_d through the SG relief valve and the cladding surface temperature in the cases of the C_d values of 0.74, 0.84, and 0.94 (Fig. 13).

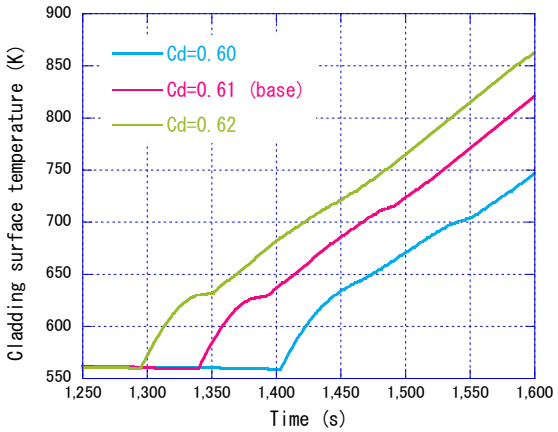

Fig. 9 Discharge coefficient through break versus cladding surface temperature by sensitivity analysis

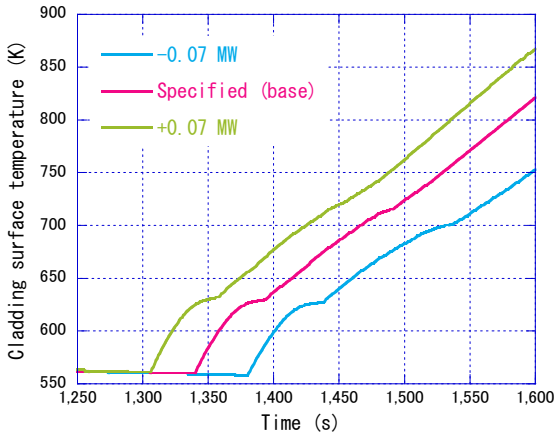

Fig. 10 Core decay power versus cladding surface temperature by sensitivity analysis

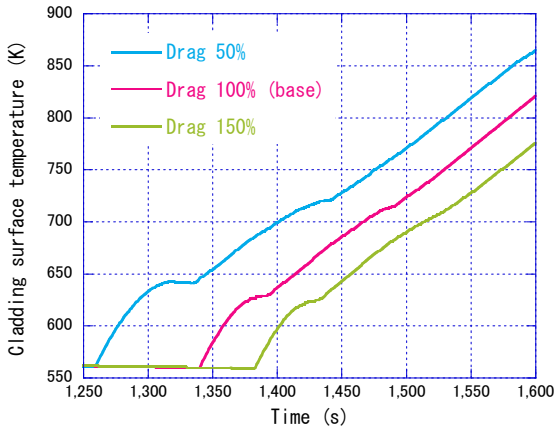

Fig. 11 Gas-liquid inter-phase drag in core versus cladding surface temperature by sensitivity analysis

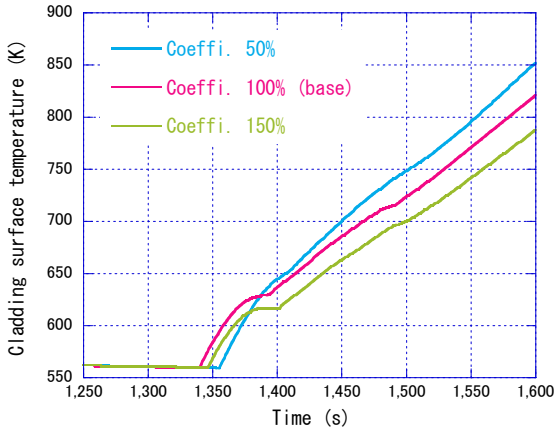

Fig. 12 Film boiling and steam convective heat transfer coefficients in core versus cladding surface temperature by sensitivity analysis

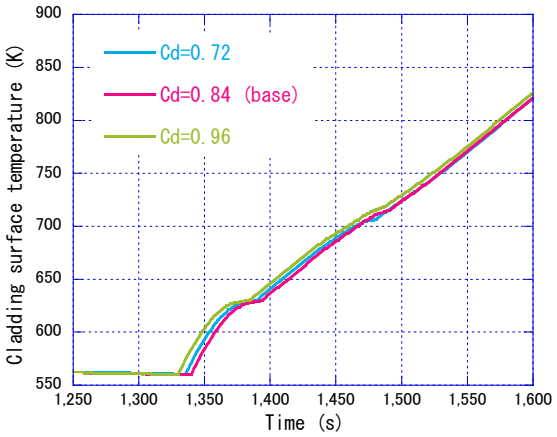

Fig. 13 Discharge coefficient through SG relief valve versus cladding surface temperature by sensitivity analysis

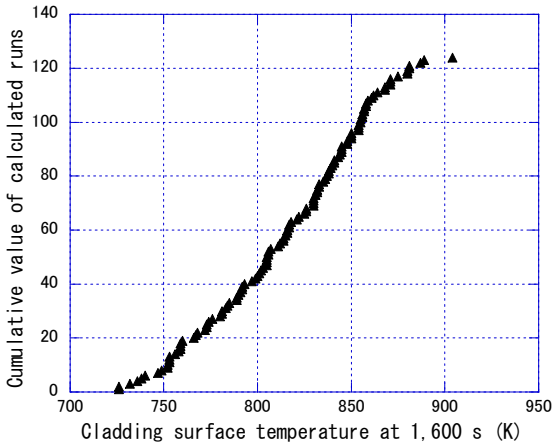

Fig. 14 Relationship between cladding surface temperature at 1,600 s and cumulative value of calculated runs

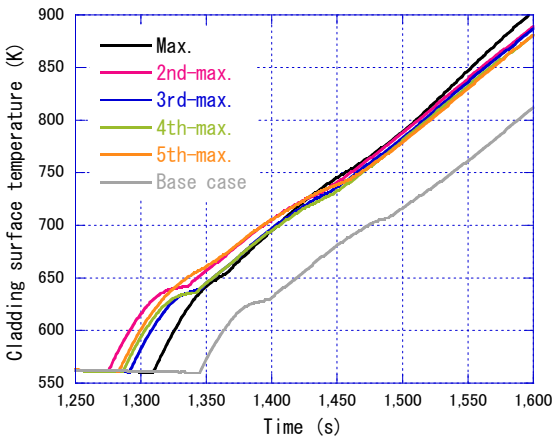

Fig. 15 Calculated results of order statistics for maximum to fifth-maximum cladding surface temperatures at 1,600 s

Fig. 14 shows the relationship between the cladding surface temperature at 1,600 s and the cumulative value of the 124

calculated runs. The distribution was random for frequency at certain values of the calculated cladding surface temperature at 1,600 s. The calculated minimum and maximum cladding surface temperatures at 1,600 s were 726 K and 904 K, respectively. The experimental result of the maximum cladding surface temperature at 1,600 s was 852 K, which was a value between the calculated minimum and maximum cladding surface temperatures at 1,600 s. Fig. 15 shows the calculated results of order statistics for the maximum to fifth-maximum cladding surface temperatures at 1,600 s, which are compared to the base case calculation. Because of the 124 calculated runs depending on the order statistics, the calculated third-maximum cladding surface temperature of 887 K corresponded to a value of cladding surface temperature at 1,600 s with a 95% probability and 95% confidence level.

To identify the strength of the relationship between the two sets of data, the author applied the following Spearman's rank correlation coefficient r_s [27], that is a nonparametric measure of rank correlation depending statistically on the ranking of two variables x and y.

$$r_s = 1 - \frac{6\sum_i (x_i - y_i)^2}{n_s(n_s^2 - 1)}, \quad (3)$$

where x is the rank of the input variable (i.e. the uncertain parameter), y is the rank of the output variable (i.e. the cladding surface temperature at 1,600 s during core uncovery), and n_s is the number of data sets (i.e. 124 as the number of the calculated runs). Table IV shows the r_s values for the uncertain parameters. The r_s values for the C_d through the break, the core decay power, the core inter-phase drag, the film boiling and steam convective heat transfer coefficients in the core, and the C_d through the SG relief valve were estimated to be 0.79, 0.35, –0.37, –0.32, and –0.12, respectively. The C_d through the break was more sensitive than other uncertain parameters to the cladding surface temperature at 1,600 s because the absolute value of r_s was the largest. The C_d through the SG relief valve was poorly correlated with the cladding surface temperature at 1,600 s because the absolute value of r_s was below 0.2 [28]. The cladding surface temperature at a certain time during core uncovery thus largely depended on the combination of the uncertain parameters of the C_d through the break, the core decay power, the core inter-phase drag, and the film boiling and steam convective heat transfer coefficients in the core within the defined uncertain ranges.

TABLE IV
SPEARMAN'S RANK CORRELATION COEFFICIENTS FOR UNCERTAIN PARAMETERS

Parameter	Spearman's Rank Correlation Coefficient
Discharge coefficient through break for single-phase liquid and two-phase flow	0.79
Core decay power	0.35
Gas-liquid inter-phase drag in core	–0.37
Film boiling and steam convective heat transfer coefficients in core	–0.32
Discharge coefficient through SG relief valve	–0.12

VI. CONCLUSIONS

Post-test analysis with the RELAP5/MOD3.3 code was conducted for a ROSA/LSTF experiment simulating a PWR 1% cold leg SBLOCA without scram under the assumption of totally failed high-pressure injection system of emergency core cooling system. Sensitivity and uncertainty analyses of the LSTF test were carried out to study the influences of the defined uncertain parameters on the cladding surface temperature at a certain time during core uncovery. Major results are summarized as follows.

In the LSTF test, liquid was accumulated in the U-tube upflow-side and inlet plena of SGs during reflux condensation because of CCFL with high steam velocity. Core uncovery took place by core boil-off after the upper plenum became voided at high pressures, which induced the actuation of automatic core power reduction.

The RELAP5 code predicted the overall trends of the major thermal-hydraulic responses observed in the LSTF test well. The break flow rate, however, was overpredicted during two-phase flow discharge period, probably due to insufficient prediction of the cold leg liquid level during two-phase NC and reflux condensation. Some discrepancies from measured data appeared in the liquid levels at the hot leg, the SG U-tube upflow-side and inlet plena, and the core.

The author created the PIRT for each component from the viewpoint of the importance of phenomena in determining the cladding surface temperature at a certain time during core uncovery, on the basis of the experimental data analysis and the post-test analysis. The author clarified the cladding surface temperature at a certain time during core uncovery was largely influenced by the combination of the uncertain parameters of the C_d through the break, the core decay power, the core inter-phase drag, and the film boiling and steam convective heat transfer coefficients in the core within the defined uncertain ranges.

ACKNOWLEDGMENT

The author would like to thank Messrs. M. Ogawa and A. Ohwada of Japan Atomic Energy Agency for performing the LSTF test under collaboration with members from Nuclear Engineering Co. as well as Miss K. Toyoda of Research Organization for Information Science and Technology for manipulating the LSTF test data.

REFERENCES

[1] USNRC, "Through-wall circumferential cracking of reactor pressure vessel head control rod drive mechanism penetration nozzles at Oconee nuclear station, Unit 3," NRC Information Notice 2001-05, USNRC, Washington, DC, 2001.

[2] A. Cuadra, J. Ragusa, T. Downar, and K. Ivanov, "Analysis of a CRDM nozzle break LOCA without scram using the U.S. NRC coupled code TRAC-M/PARCS," in *Proc. of the 10th International Conference on Nuclear Engineering (ICONE-10)*, Arlington, USA, April 2002.

[3] The ROSA-V Group, "ROSA-V Large Scale Test Facility (LSTF) System Description for the Third and Fourth Simulated Fuel Assemblies," JAERI-Tech 2003-037, Japan Atomic Energy Research Institute, Ibaraki, Japan, 2003.

[4] T. Takeda, H. Asaka, and H. Nakamura, "Analysis of the OECD/NEA ROSA Project experiment simulating a PWR small break LOCA with

high-power natural circulation," Ann. Nucl. Energy, vol. 36, 2009, pp. 386–392.
[5] USNRC Nuclear Safety Analysis Division, "RELAP5/MOD3.3 Code Manual," NUREG/CR-5535/Rev 1, Information Systems Laboratories, Inc., 2001.
[6] V. Martinez, F. Reventós, and C. Pretel, "Post-test calculation of the ROSA/LSTF Test 3-1 using RELAP5/Mod3.3," NUREG/IA-0409, USNRC, Washington, DC, 2012.
[7] S. Gallardo, V. Abella, G. Verdú, and A. Querol, "Assessment of TRACE 5.0 against ROSA Test 3-1, cold leg SBLOCA," NUREG/IA-0413, Washington, DC, 2012.
[8] N. Zuber, "Problems in Modeling Small Break LOCA," NUREG-0724, USNRC, Washington, DC, 1980.
[9] V.G. Zimin, H. Asaka, Y. Anoda, and M. Enomoto, "Verification of J-TRAC code with 3D neutron kinetics model SKETCH-N for PWR rod ejection analysis," in *Proc. of the 9th International Topical Meeting on Nuclear Reactor Thermal Hydraulics (NURETH-9)*, San Francisco, USA, October 1999.
[10] H.K. Fauske, "The discharge of saturated water through tubes," AlChE Symp. Ser., vol. 61, 1965, pp. 210–216.
[11] K.H. Ardron and R.A. Furness, "A study of the critical flow models used in reactor blowdown analysis," Nucl. Eng. Des., vol. 39, 1976, pp. 257–266.
[12] D.W. Sallet, "Thermal hydraulics of valves for nuclear applications," Nucl. Sci. Eng., vol. 88, 1984, pp. 220–244.
[13] G.B. Wallis, "One-Dimensional Two-Phase Flow," McGraw-Hill Book, New York, USA, 1969.
[14] T. Yonomoto, Y. Anoda, Y. Kukita, and Y. Peng, "CCFL characteristics of PWR steam generator U-tubes," in *Proc. of the ANS International Topical Meeting on Safety of Thermal Reactors*, American Nuclear Society, Portland, Ore, USA, July 1991.
[15] T. Takeda, A. Ohnuki, and H. Nishi, "RELAP5 code study of ROSA/LSTF experiments on PWR safety system using steam generator secondary-side depressurization," J. Energy Power Eng., vol. 9, 2015, pp. 426–442.
[16] M. Ishii and K. Mishima, "Study of Two-fluid Model and Interfacial Area," NUREG/CR-1873, Argonne National Laboratory, Lemont, IL, 1980.
[17] H. Kumamaru, Y. Kukita, H. Asaka, M. Wang, and E. Ohtani, "RELAP5/MOD3 code analyses of LSTF experiments on intentional primary-side depressurization following SBLOCAs with totally failed HPI," Nucl. Technol., vol. 126, 1999, pp. 331–339.
[18] L.A. Bromley, "Heat transfer in stable film boiling," Chem. Eng. Prog., vol. 46, 1950, pp. 221–227.
[19] K.H. Sun, J.M. Gonzalez-santalo, and C.L. Tien, "Calculations of combined radiation and convection heat transfer in rod bundles under emergency cooling conditions," J. Heat Transfer, vol. 98, 1976, pp. 414–420.
[20] F.W. Dittus and L.M.K. Boelter, "Heat transfer in automobile radiators of the tubular type," Int. Comm. Heat Mass Transfer, vol. 12, 1985, pp. 3–22.
[21] J.R. Sellars, M. Tribus, and J.S. Klein, "Heat transfer to laminar flows in a round tube or flat conduit: the Graetz problem extended," Transactions of the ASME, vol. 78, 1956, pp. 441–448.
[22] S.W. Churchill and H.H.S. Chu, "Correlating equations for laminar and turbulent free convection from a vertical plate," Int. J. Heat Mass Transfer, vol. 18, 1975, pp. 1323–1329.
[23] A. Guba, M. Makai, and L. Pál, "Statistical aspects of best estimate method–I," Reliability Eng. Syst. Safety, vol. 80, 2003, pp. 217–232.
[24] A. de Crécy, P. Bazin, H. Glaeser, et al., "Uncertainty and sensitivity analysis of the LOFT L2-5 test: Results of the BEMUSE programme," Nucl. Eng. Des., vol. 238, 2008, pp. 3561–3578.
[25] R.L. Iman and M.J. Schortencarier, "A FORTRAN program and user's guide for the generation of Latin hypercube and random samples for use with computer models," NUREG/CR-3624, USNRC, Washington, DC, 1984.
[26] A. Yamamoto, K. Kinoshita, T. Watanabe, and T. Endo, "Uncertainty quantification of LWR core characteristics using random sampling method," Nucl. Sci. Eng., vol. 181, 2015, pp. 160–174.
[27] W.W. Daniel, "Spearman rank correlation coefficient," Applied Nonparametric Statistics (second ed.), PWS-Kent Publishing, Boston, MA, 1990.
[28] J. Freixa, T.W. Kim, and A. Manera, "Post-test thermal-hydraulic analysis of two intermediate LOCA tests at the ROSA facility including uncertainty evaluation," Nucl. Eng. Des., vol. 264, 2013, pp. 153–160.

Takeshi Takeda is on loan to Nuclear Regulation Authority from Japan Atomic Energy Agency. His interests include thermal-hydraulic safety during accidents and abnormal transients of light water reactor through experiments using test facilities and by calculations with best-estimate computer code.